Published in final edited form as:

Nature. 2017 March 30; 543(7647): 738–741. doi:10.1038/nature21414.

Energy Transduction and Alternating Access of the Mammalian ABC Transporter P-glycoprotein

Brandy Verhalen[1,4,*], **Reza Dastvan**[1,*], **Sundarapandian Thangapandian**[2], **Yelena Peskova**[3], **Hanane A. Koteiche**[1], **Robert K. Nakamoto**[3], **Emad Tajkhorshid**[2], and **Hassane S. Mchaourab**[1,§]

[1]Department of Molecular Physiology and Biophysics, Vanderbilt University, Nashville, Tennessee 37232, USA

[2]Department of Biochemistry, Center for Biophysics and Quantitative Biology, and Beckman Institute for Advanced Science and Technology, University of Illinois at Urbana-Champaign, Urbana, Illinois 61801, USA

[3]Department of Molecular Physiology and Biological Physics, University of Virginia, Charlottesville, Virginia 22908, USA

ATP binding cassette (ABC) transporters of the exporter class harness the energy of ATP hydrolysis in the nucleotide binding domains (NBDs) to power the energetically uphill efflux of substrates by a dedicated transmembrane domain (TMD)[1-4]. Although numerous investigations have described the mechanism of ATP hydrolysis and defined the architecture of ABC exporters, a detailed structural dynamic understanding of the transduction of ATP energy to the work of substrate translocation remains elusive. Here we utilized double electron-electron resonance (DEER)[5-6] and molecular dynamics (MD) simulations to describe the ATP- and substrate-coupled conformational cycle of the mammalian ABC efflux transporter P-glycoprotein (Pgp), or ABCB1, which plays a central role in the clearance of xenobiotics and in cancer resistance to chemotherapy[7]. Pairs of spin labels were introduced at residues selected to track the putative inward-facing (IF) to outward-facing (OF) transition. Our findings illuminate how ATP energy is harnessed in the NBDs in a two-stroke cycle and elucidate the consequent conformational motion that reconfigures the TMD, two critical aspects of Pgp transport mechanism. Along with a fully atomistic model of the OF conformation in membranes, the insight into Pgp conformational dynamics harmonizes mechanistic and structural data into a novel perspective on ATP-coupled transport and reveal mechanistic divergence within the efflux class of ABC transporters.

§Correspondence and requests for materials should be addressed to H.S.M (hassane.mchaourab@vanderbilt.edu).
4Current address: Department of Pediatrics, University of Texas Southwestern Medical Center, Dallas, Texas 75390, USA
*These authors contributed equally to this work.

Supplementary Information is linked to the online version of the paper at www.nature.com/nature.

Author Contributions: H.S.M., B.V., and R.K.N. designed the experimental studies. B.V. and R.D. purified the mutants and performed the experiments. R.D. and B.V. analyzed the data. S.T. and E.T. designed and performed the molecular dynamics simulations. H.S.M, R.D., B.V., S.T., and E.T. wrote the paper. Y.P. cloned and expressed the mutants. H.A.K. and B.V. initially contributed in the optimization, cloning and expression of Pgp.

Structural mechanism of Pgp alternating access

To derive a global view of the conformational dynamicsunderpinning Pgp transport, we carried out distance measurements under biochemical conditions which stabilize specific intermediates (Fig. 1). Spin-labeled mutants, showing robust substrate-stimulated ATP turnover (Extended Data Fig. 1), were analyzed by DEER in mixed lipid/detergent micelles in the ligand-free (Apo) state, in the presence of the ATPase-stimulating substrate verapamil (Ver)[8], in the presence of AMP-PNP/Mg^{2+}/Ver to mimic the ATP/substrate-bound intermediate, following addition of vanadate (Vi) and ATP/Mg^{2+} (referred to ADP-Vi-Ver in Fig. 1) to trap the high-energy post hydrolysis intermediate, hereafter referred to as the transition state of ATP hydrolysis[9-10], and in the presence of ADP/Mg^{2+}/Ver to populate the low energy post-hydrolysis intermediate. Pgp alternating access under turnover conditions was investigated in the presence of excess ATP/Mg^{2+} as prevalent in the cell.

We observed extensive conformational movements only in the transition state of ATP hydrolysis (Fig. 1 and Extended Data Figs. 2 and 3 and SI) trapped by Vi. Distance distributions reveal a pattern of changes that is consistent with an ATP-hydrolysis powered isomerization of Pgp from an IF conformation to an OF-like conformation along the lines of the MsbA model of alternating access[11,12]. A closing motion of the NBDs and intracellular side of the TMD is gleaned from the consistently shorter distributions in the transition state relative to the Apo state (Fig. 1b and 1c). In contrast, the appearance of longer distance components reveals concomitant opening of the extracellular side (Fig. 1d and Extended Data Fig. 3, see supplementary results and discussion for details). Furthermore, the alternating access of the TMD involves the swapping of helices that were part of one TMD leaflet in the IF conformation to the other leaflet in the OF conformation. For instance, the MsbA model[11,12] predicts that TMs 5 and 6 as well as TMs 11 and 12 are closer in the OF conformation on the intracellular side, precisely the distance changes observed experimentally (Fig. 1c and Extended Data Fig. 3).

Distance distributions on the intracellular side in the apo state often have average distances larger than those expected by modeling the spin labels on mouse Pgp crystal structure[13,14] (Fig. 1b and 1c) suggesting a more open IF conformation similar to that observed in the *C. elegans* Pgp[15] structure. Pairs of labels at the C terminus of the NBDs report shorter than expected distances between the spin labels suggesting a highly flexible region undergoing independent motion relative to the NBD (Fig. 1b). This result is consistent with spontaneous disulfide cross-link of the corresponding cysteine pairs (Extended Data Fig. 2)[16].

Broad and overlapping distance distributions on the extracellular side in the transition state indicate the co-existence of IF and OF conformations (Fig. 1d) whereas the distance distributions were mostly single population on the intracellular side. Thus, ATP hydrolysis drives Pgp to a transition state which is homogenous on the intracellular side but heterogeneous on the extracellular side.

The NBDs form an asymmetric two-cylinder engine

Dimerization of the NBDs[11,12] leads to the assembly of two nucleotide binding sites (NBSs), each sandwiched between the Walker A motif of one NBD and the ABC signature motif of the other[17]. Therefore, we monitored the NBSs conformational dynamics using structurally equivalent spin label pairs monitoring similar locations for each NBS. While the short-distance component, expected based on the OF conformations of MsbA[11,12] and Sav1866[18], were observed in the transition state (Fig. 2), distance distributions were asymmetric for pairs 400/1156 at NBS1 and 511/1043 at NBS2 (Fig. 3b). Unique to these pairs are residues (400 and 1043) adjacent to the "A-loop" which directly interacts with the adenosine moiety of bound ATP through a tyrosine[19]. A short-distance component (population 50%) is exclusively observed for the A-loop pair monitoring NBS2, whereas minor changes in the distance distributions were observed for the equivalent pair at NBS1 (Fig. 3b and Extended Data Fig. 4) in the transition state. Thus, there is an intrinsic local structural asymmetry at the NBSs of Pgp in the transition state.

To identify the mechanistic origin of NBS asymmetry, we mutated the conserved catalytic glutamates, E552 (NBS1) and E1197 (NBS2), which polarize and orient a water molecule in line for a nucleophilic attack on the γ-phosphate of ATP[20-24]. The E552Q and E1197Q mutations, which were shown to impair ATP turnover (Extended Data Fig. 1c)[22-23], invert the structural asymmetry of the NBSs (Fig. 3 and Extended Data Figs. 4 and 5). In the E1197Q (NBS2) background, a short-distance component appears at the A-loop pair of NBS1 concomittant with a substantial reduction in its population at the corresponding pair of NBS2 (Fig. 3 and Extended Data Fig. 4). Other spin label pairs monitoring the NBSs do not show asymmetry in their distance distributions pinpointing the A-loop as a sensor of asymmetric catalysis by Pgp (Extended Data Fig. 5).

Either E to Q mutation stabilizes the transition state under turnover conditions (excess ATP/Mg^{2+}) as evidenced by distance distributions reflecting the formation of the NBD dimer and alternating access of the TMD (Extended Data Figs. 4-6) whereas observation of the short-distance component in the A-loop pairs requires vanadate trapping. Only in the two glutamate substitutions background are near-equal populations of the short-distance component observed under turnover conditions (Fig. 3e). Because the double E to Q mutant was shown to trap nucleotides with high affinity at both NBSs[21], we conclude that the short-distance component of the A-loop pairs is a signature of a bound and occluded ATP. Together, these findings are consonant with evidence of ATP turnover by one NBS at a time, the alternating-site hydrolysis model[25,26], and catalytic inequivalence of the NBSs[20].

A novel model of Pgp OF conformation

To frame the movements described above in a structural context, we modeled the OF conformation using a novel approach described in SI with the goal of producing a stable model that will have the structural features expected for an OF state in a lipid bilayer (Fig. 4a-c, Extended Data Figs. 7-8, Extended Data Tables 1-2, and SI). Conventional modeling approaches consistently resulted in models that depart from the expected OF conformation within 10s of nanoseconds of simulations. Therefore, specific structural elements, previously

demonstrated to control the alternating access mechanism[27], were used as metrics for the stability of the model (Extended Data Fig. 8c and 8d). Our nonequilibrium modeling approach resulted in a closed intracellular and stably open extracellular sides for the OF conformation (See SI). Simulations with several variations of the nonequilibrium protocols (Extended Data Table 1) unveiled key features necessary for the stabilization of Pgp OF conformation. Specifically, the OF model displays an intracellular closing distance of 8.8 Å compared to 8.9 Å and 9.3 Å observed in MsbA[11] and Sav1866[18], respectively (Extended Data Fig. 8e). A fluctuating trend between 28 Å and 30 Å (Extended Data Fig. 8f) demonstrates a dynamic and flexible extracellular opening. Remarkably, we found a close agreement between the distances predicted by this model and the experimental DEER in the transition state (Extended Data Figs. 2-6). Thus, Pgp transition state has structural characteristics of an OF conformation similar to that of MsbA[11,12] and Sav1866[18]. However, the DEER data as well as the simulations reveal conformational flexibility at the extracellular side which arise from a relatively large number of proline and glycine residues in the TM regions as we suggested previously[28]. Finally, the model does not capture the NBS asymmetry due to the use of MsbA symmetric OF conformation as a template.

A model of energy transduction by Pgp

A novel model of Pgp conformational cycle grounded in existing mechanistic data emerges from our findings (Fig. 4d). While Pgp must undergo large amplitude movements that dimerize the NBDs to enable ATP hydrolysis, the observation of Apo-like distance distributions in the presence of excess ATP/Mg^{2+} demonstrates that stabilization of the OF conformation requires ATP hydrolysis. Furthermore, it implies that Pgp promptly resets to the IF conformation following hydrolysis, i.e., the OF state is short-lived. Therefore, most Pgp molecules in the cell are inward-facing poised to bind substrates. This is in stark contrast to MsbA where ATP binding locks the transporter in the OF conformation[29] and may reflect an intrinsic difference in the rate limiting step of transport between MsbA and Pgp.

Despite intact ATP hydrolysis motifs in Pgp, we uncovered local structural asymmetry at the NBSs that is associated with reported catalytic asymmetry[20,22,24]. The transition state of Pgp is heterogeneous consisting of at least two equally populated conformations distinguished by the structure of the A-loop and the opening of the TMD extracellular side. We propose that in one conformation NBS2 clamps down on an occluded ATP while NBS1 has turned its ATP over (3 in Fig. 4d). In the other conformation, both NBSs have hydrolyzed ATP and the A-loop at NBS2 is released (4) concomitant with substrate extrusion. Thus, occlusion of nucleotide occurs in one NBS at a time and the NBSs take turns in hydrolysis, but there is an intrinsic catalytic preference most likely for NBS1 since nucleotide occlusion was only detectable at NBS2 in WT Pgp.

That hydrolysis of a single ATP molecule is sufficient for closing the intracellular side is demonstrated by its homogeneous conformation in the transition state. In contrast, opening of the extracellular side must require the hydrolysis of two ATP molecules; as a result, its conformation is heterogeneous. This implies the population of a doubly occluded conformation of the TMD following hydrolysis of the first ATP molecule (3 in Fig. 4d). The

structure of this conformation which has not been reported previously requires the flexibility of Pgp TMD noted in the MD simulations[28]. We propose that drug extrusion requires a two-stage hydrolysis to ensure the translocation of bound substrate to the extracellular milieu[1].

Our findings demonstrate a similar outline of Pgp alternating access to that of MsbA and the heterodimeric transporter BmrCD[29] but is driven by a divergent mechanism of energy input and transduction. Asymmetric ATP hydrolysis as well as different coupling between domains predict a spectrum of transport mechanisms. Delineation of the sequence determinants and the physiological consequences of this mechanistic divergence is the next central question.

Methods

No statistical methods were used to predetermine sample size.

Cloning

The mouse ortholog of P-glycoprotein, *mdr3,* was cloned by standard molecular biology techniques from pHIL-D2-mdr3CL, a *P. pastoris* expression construct generously donated by I.L. Urbatsch into pFastBac-1 with a C-terminal 10×His tag. This construct has the nine native cysteines replaced by alanines as previously described and characterized[30]. Point mutations for site-directed spin labeling and mutations of catalytic residues were created by site directed mutagenesis by QuikChange®. Validity of mutations was confirmed by sequencing.

Expression

Cysless (CL) and double-cys mutants were expressed using standard protocols from Invitrogen and the pFastBac system. Sf21 cells were infected at ~2.0×10^6 cells/ml with an estimated multiplicity of infection of 3 for 66-72 hours at 27°C in a shaking incubator in 2L disposable flasks. 0.25% of FBS was added at 24 hours post infection. Cells were harvested by centrifugation and stored at -80°C. Double cys pairs 607-1252, 615-1276 and 613-1258 were expressed and purified as previously described[28].

Membrane isolation

Cell pellets were thawed and resuspended in Low Salt Lysis Buffer (50 mM NaCl, 50 mM Tris-HCl, 0.5 mM EDTA, 0.5 mM EGTA, pH 7.4 at room temperature (RT)) and protease inhibitors were added and the cell suspension was lysed via sonication. Cell debris was pelleted by centrifugation at 9,000 × g for 30 min at 4°C. 2 mM dithiothreitol (DTT) was added to supernatant, and membranes were separated by centrifugation at 138,000 × g for 75 min at 4°C. Membranes were washed by resuspension by dounce homogenizer in 30 ml Membrane Wash Buffer (50 mM Tris-HCl, 10% glycerol (v/v), pH 7.4 at 4°C). Membranes were pelleted by centrifugation at 138,000 × g for 45 min at 4°C. Membrane pellets were resuspended by dounce homogenizer in Buffer A (50 mM Tris-HCl, 50 mM NaCl, 30% glycerol (v/v), 10 mM imidazole, pH 7.4 at 4°C) with protease inhibitors and 2 mM DTT.

Purification and spin labeling

Buffer A was added to a final volume of 0.058 g membranes/ml, supplemented by n-dodecyl-β-d-maltopyranoside (β-DDM) and DTT to a final concentration of 1.25% and 1 mM, respectively. Solution was stirred on ice for 1 h. Insoluble material was pelleted by centrifugation at 80,000 × g for 30 min at 4°C. Supernatant was incubated with 2 ml Ni-NTA resin (Qiagen) for 2 h with rocking at 6°C. Resin was packed into a gravity flow column at 6°C. Nonspecific proteins were washed away with one column volume (CV) of Buffer A + 0.1% β-DDM and 10 CV 30 mM Wash Buffer (Buffer A except 30 mM imidazole) + 0.1% β-DDM. Pgp was eluted from the Ni-NTA with Buffer B + 0.1% β-DDM (50 mM Tris-HCl, 50 mM NaCl, 20% glycerol (v/v), 300 mM imidazole, pH 7.4 at 4°C). Protein concentration was estimated by absorbance at 280 nm with a predicted extinction coefficient of 115,600 M^{-1}• cm^{-1}. The pH of purified Pgp was decreased to 7.0 by addition of 7% by volume of 1 M MES. 40-fold excess of (1-Oxyl-2,2,5,5-tetramethylpyrroline-3-methyl) Methanethiosulfonate (MTSSL) was added followed by two additions of 20-fold excess after 1.5 h and 1 h incubation. Labeling additions were carried out on ice, and the reaction was continued overnight. Purified Pgp, identified by SDS-PAGE, was concentrated ~12-14 fold using Amicon Ultra-50 kDa centrifugal filters (Millipore). The spin-labeled Pgp was then separated from excess spin label and free micelles by size exclusion chromatography in Gel Filtration Buffer (50 mM Tris-HCl, 50 mM NaCl, 20% glycerol (v/v), 0.05% βDDM pH 7.4 at 4°C). Purified Pgp was identified by SDS-PAGE and concentrated 30-40 fold with a Ultra-100 kDa centrifugal filter. Pgp sample preparation was as described before with 7 minutes incubation at 37°C for DEER spectroscopy[28]. The molar ratio of protein:lipid:detergent is 1:105:12.7. The lipids were suspended in Tris buffer (pH 6.9) as a mixture (3:2 *E. coli* polar lipids:phosphatidylcholine) to a final concentration of 50 mg/ml. Protein, extra β-DDM in gel filtration buffer and lipids were mixed until homogeneous. Nucleotides and substrates were then subsequently mixed in and incubated. The final concentrations of ATP (or AMP-PNP), vanadate, $MgSO_4$, and verapamil were 5 mM, 1 mM, 5 mM, and 0.2 mM, respectively. Mg^{2+} is included in all samples containing nucleotide.

The experiments were not randomized. The investigators were not blinded to allocation during experiments and outcome assessment.

ATPase assay

The specific ATPase activity of Pgp was determined by a hydrolyzed phosphate assay as previously described[31] with the following modifications. 6-8 μg of Pgp with an equal amount (w/w) of *E. coli* lipids were incubated for 10 min at 37°C in three conditions of increasing amounts of ATP: basal (no substrate), 200 μM verapamil (stimulated) and 200 μM verapamil with 1 mM vanadate (vanadate inhibited) (two repeats each). The reaction was stopped by adding 1 volume of 10% SDS and color was developed using a 1:1 solution of ammonium molybdate (2% in 1M HCl) and ascorbic acid (12% in 1 M HCl). The absorbance at 850 nm was measured on a BioTek Synergy H4 microplate reader. The amount of phosphate hydrolyzed was determined by comparison to inorganic phosphate standards.

CW EPR and DEER spectroscopy and data analysis

DEER spectroscopy was performed on an Elexsys E580 EPR spectrometer operating at Q-band frequency (33.9 GHz) equipped with a 10W Amp-Q amplifeier (Bruker) with the dead-time free four-pulse sequence at 83 K[32]. The pulse lengths were 10 ns ($\pi/2$) and 20 ns (π) for the probe pulses and 40 ns for the pump pulse. The frequency separation was 63 MHz. For CW-EPR on the DEER samples after DEER data collection, spectra were collected on a Bruker EMX spectrometer. Primary DEER decays were analyzed using home-written software operating in the Matlab environment[29]. Briefly, the software carries out global analysis of the DEER decays obtained under different conditions for the same spin-labeled position. The distance distribution is assumed to consist of a sum of Gaussians, the number of which is determined based on a statistical criterion. Distance distributions on the X-ray structure (PDB accession 4M1M)[14] and OF model were predicted *in silico* using a rotamer library approach by MMM 2013.2 software package[33]. Rotamer library calculations were conducted at 298 K.

Structural modeling for MD simulations

An OF model was constructed using MsbA[11], a bacterial ABC exporter, as a structural template with Modeller 9v12 program[34]. Sequences of mouse Pgp and MsbA were aligned based on their secondary structure details using PRALINE[35,36]. The improperly built TM1/TM2 and TM7/TM8 connecting tips were rebuilt as observed in crystallographically solved IF state (PDB accession 4M1M)[14] (Extended Data Fig. 7). The Mg^{2+} and ATP molecules were docked in to the NBDs based on the crystal structure of dimerized NBDs of HlyB, an ABC transporter (PBD accession 1XEF)[37]. A detailed description of the steps involved in structural modeling is provided in Supplemental Information.

MD simulations

All simulations were performed at atomic resolution using NAMD2[38] with CHARMM36 force field[39-41]. A complete neutralized system of ~220,000 atoms was built employing the Membrane Builder tool[42-44] of CHARMM-GUI[45-46]. Non-equilibrium simulations with different combinations of a set of specific collective variables were performed for 30 ns to form key NBD-NBD interactions and a central salt bridge in the TMD, and to restrain the extracellular opening followed by extended simulations with no bias (Extended Data Table 1). More detailed descriptions of the simulation protocols employed in the present study are provided in Supplemental Information.

The datasets generated during and/or analysed during the current study are available from the corresponding author on reasonable request.

Extended Data

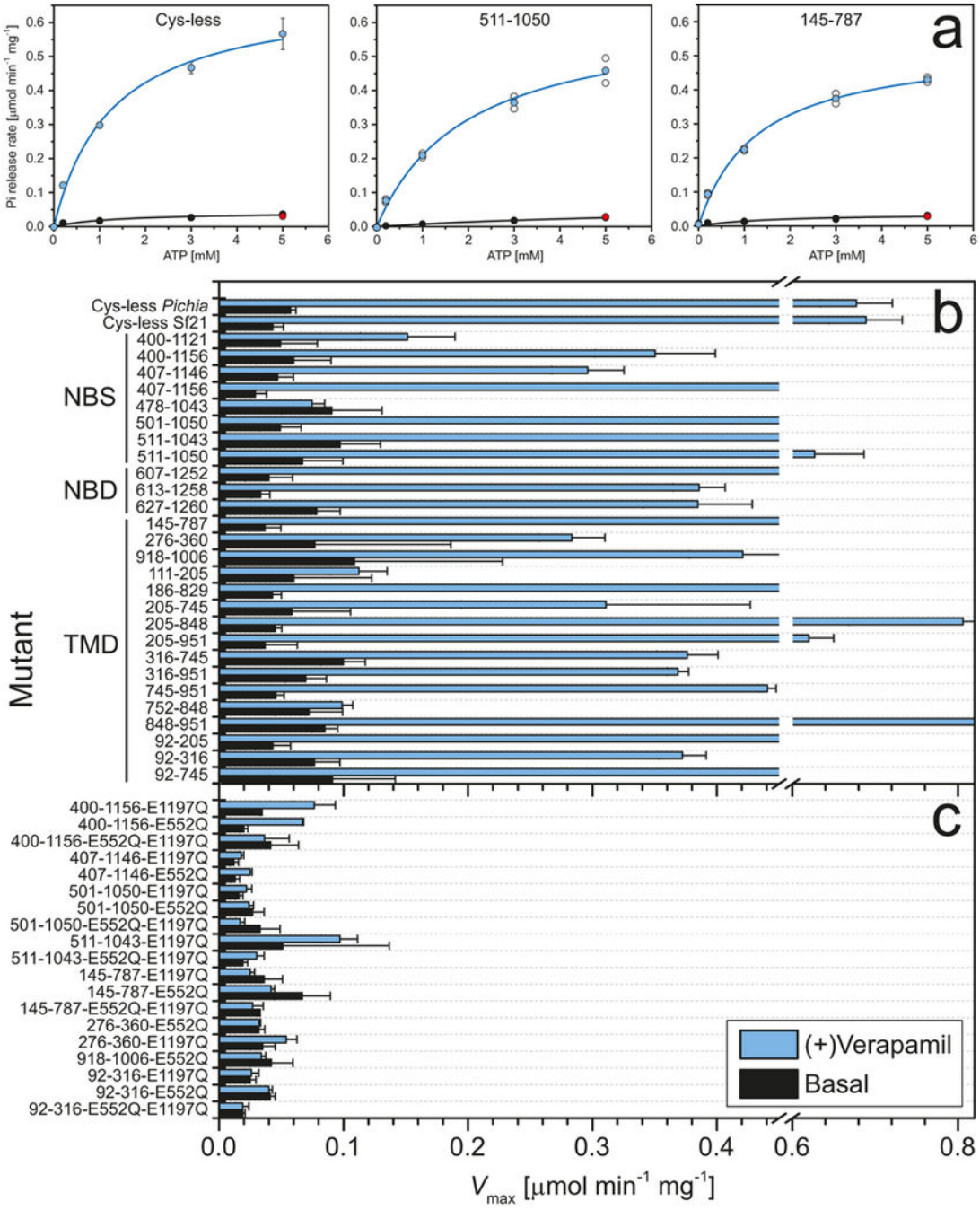

Extended Data Figure 1. ATPase activity

(a) The representative ATPase assays on Pgp mutants. Basal (black) and verapamil-stimulated (blue) ATP hydrolysis were measured by Pi-release. The red dots represent the release rate under vanadate trapping condition (5 mM ATP, 1 mM vanadate). The maximum activity (V_{max}) values for mutants with intact NBSs (b) and with catalytic glutamate

substitutions (c) are determined by fitting the data with simple Michaelis-Menten equation. Error bars are fitting errors or standard deviation (cys-less Pgp).

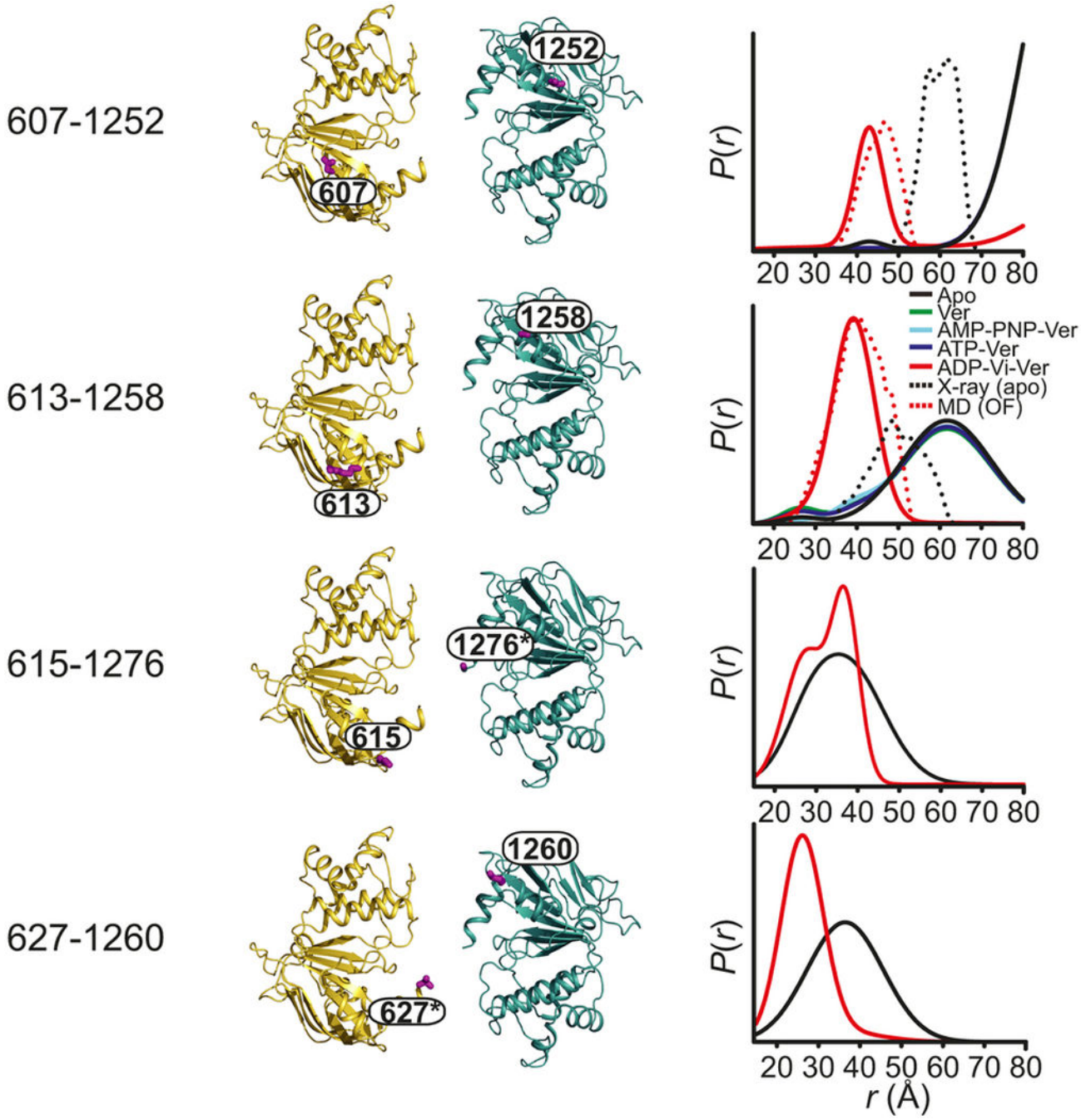

Extended Data Figure 2. NBDs form a closed dimer in the vanadate-trapped transition state

From left to right, ribbon representation of NBDs viewed from cytosolic side (PDB accession 4M1M) with residues mutated to cysteine represented as purple sticks, and DEER distance distributions. Inward-facing and outward-facing distance distributions predicted from the X-ray structure of the IF, and from the OF model are shown as dotted black and red

traces respectively. Residues 627 and 1276 were not resolved in the X-ray structure. Tha data sets on spin-labeled pairs 607-1252 and 613-1258 are repeated from main Figure 1b.

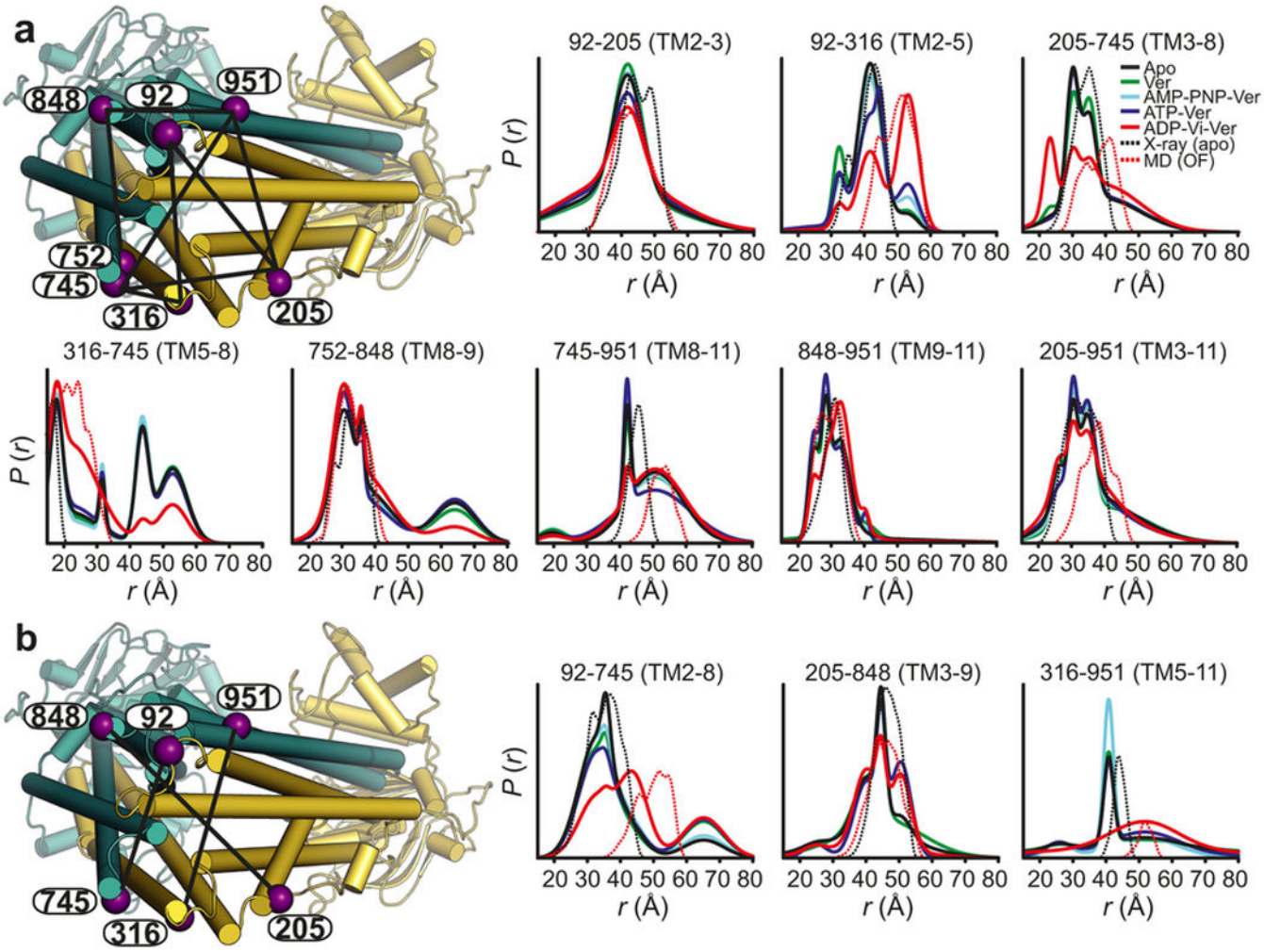

Extended Data Figure 3. Opening of the extracellular side of the TMD in the transition state

Spin-labeled pairs designed to monitor distances between structurally nonequivalent helices (a) as well as equivalent helices (b) in the two leaflets are represented as purple spheres. Changes in the distance distributions are predominantly indicative of increased distances as predicted by the MsbA OF structure and consistent with Pgp OF model. However, even for residues where distance changes are observed, the distributions are broad and components similar to those of the Apo state are present suggesting a heterogeneous transitions state. Inward-facing and outward-facing distance distributions predicted from the X-ray structure of the IF and from the OF model are shown as dotted black and red traces respectively.

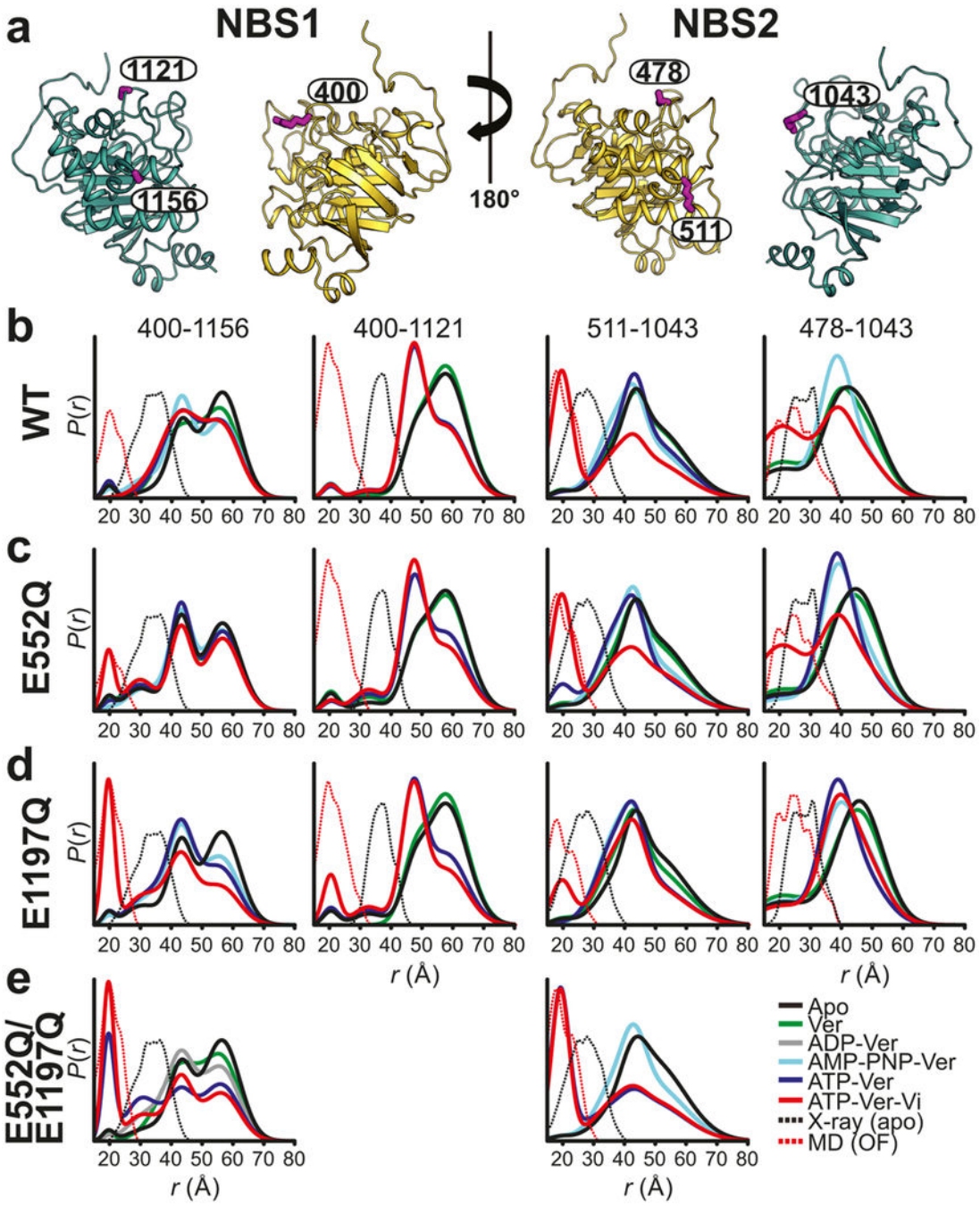

Extended Data Figure 4. Local asymmetry of the NBSs

(a) Positions of the mutated residues in each NBS are represented as purple sticks. (b-e) Distance distributions monitoring each NBS in the WT (b), E552Q (c), E1197Q (d), and E552Q/E1197Q (e) backgrounds. Spin-labeled pairs 400-1121 and 478-1043 have significantly reduced ATPase activity (see Extended Data Fig. 1). However, comparing the distributions of these spin-labeled pairs to those of 400-1156 and 511-1043, the pattern of changes in distance distributions is consistent, confirming the asymmetry is localized to the

region of the A-loop. Tha data sets on spin-labeled pairs 400-1156 and 511-1043 are repeated from main Figure 3.

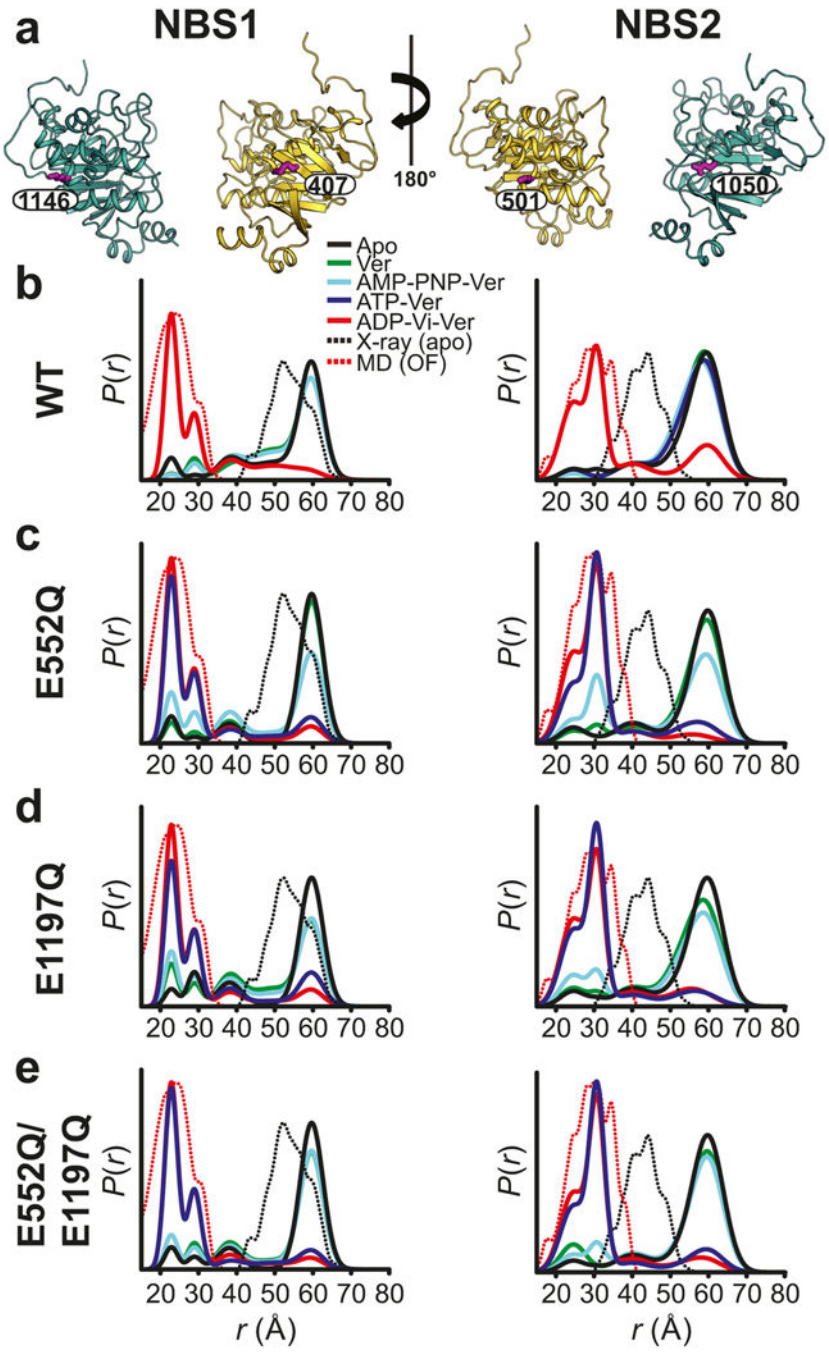

Extended Data Figure 5. Assembly of the NBSs upon vanadate-trapping of the transition state

(a) Ribbon representation of NBSs viewed from the side with the mutated residues represented as purple sticks. (b-e) Distance distributions monitoring each NBS in the WT (b), E552Q (c), E1197Q (d), and E552Q/E1197Q (e) backgrounds. The pattern and amplitude of the distance changes at these locations are similar and consistent with the

proximity of the Walker A and signature motifs in the OF conformation as previously observed for MsbA and Sav1866. Introduction of the catalytic glutamate substitutions does not affect the distance changes. Moreover, these substitutions stabilize the transitions state so that it is populated under turnover conditions- i.e in the presence of ATP/Mg^{2+} and verapamil (ATP-Ver, blue). These results demonstrate that the asymmetry identified in Supplementary Fig. 4 and its dependence on the catalytic activity of each NBS is localized to the A-loop region. The panel b is repeated from main Figure 2b.

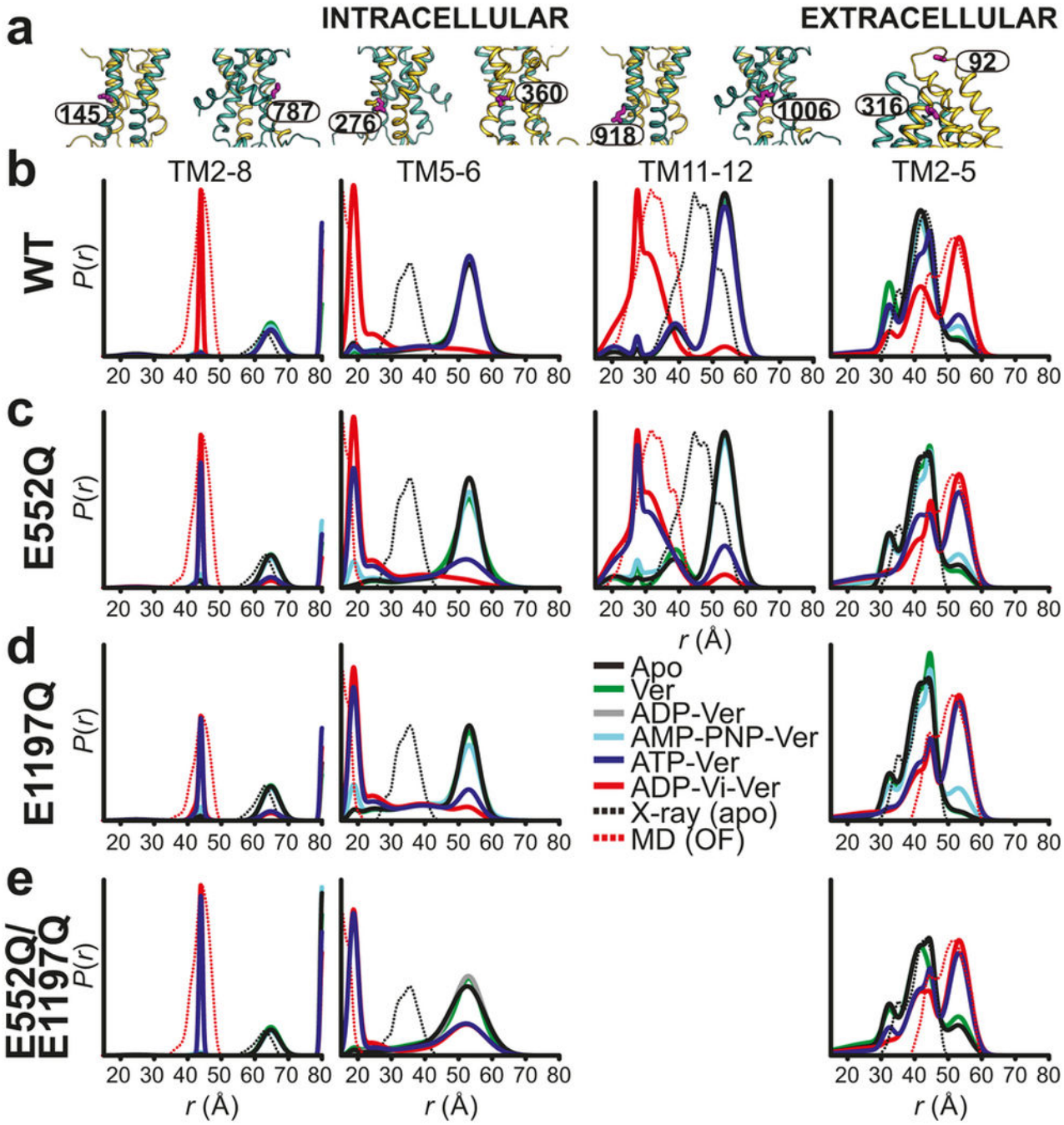

Extended Data Figure 6. The mutations of the catalytic glutamates do not alter the TMD conformational changes but stabilize the transition state

(a) Cytoplasmic (left three panels) and extracellular (right panel) TMD regions with spin labeled residues represented as purple sticks. Distance distributions monitoring cytoplasmic and extracellular closing and opening in the WT (b), E552Q (c), E1197Q (d), and E552Q/E1197Q (e) backgrounds. In the vanadate-trapped transition state (ADP-Vi-Ver, red), the distance distributions are consistent with population of the OF conformation. In the E to Q backgrounds, ATP/Mg2+ is sufficient to stabilize Pgp to OF. The panel b is repeated from main Figure 1c and 1d.

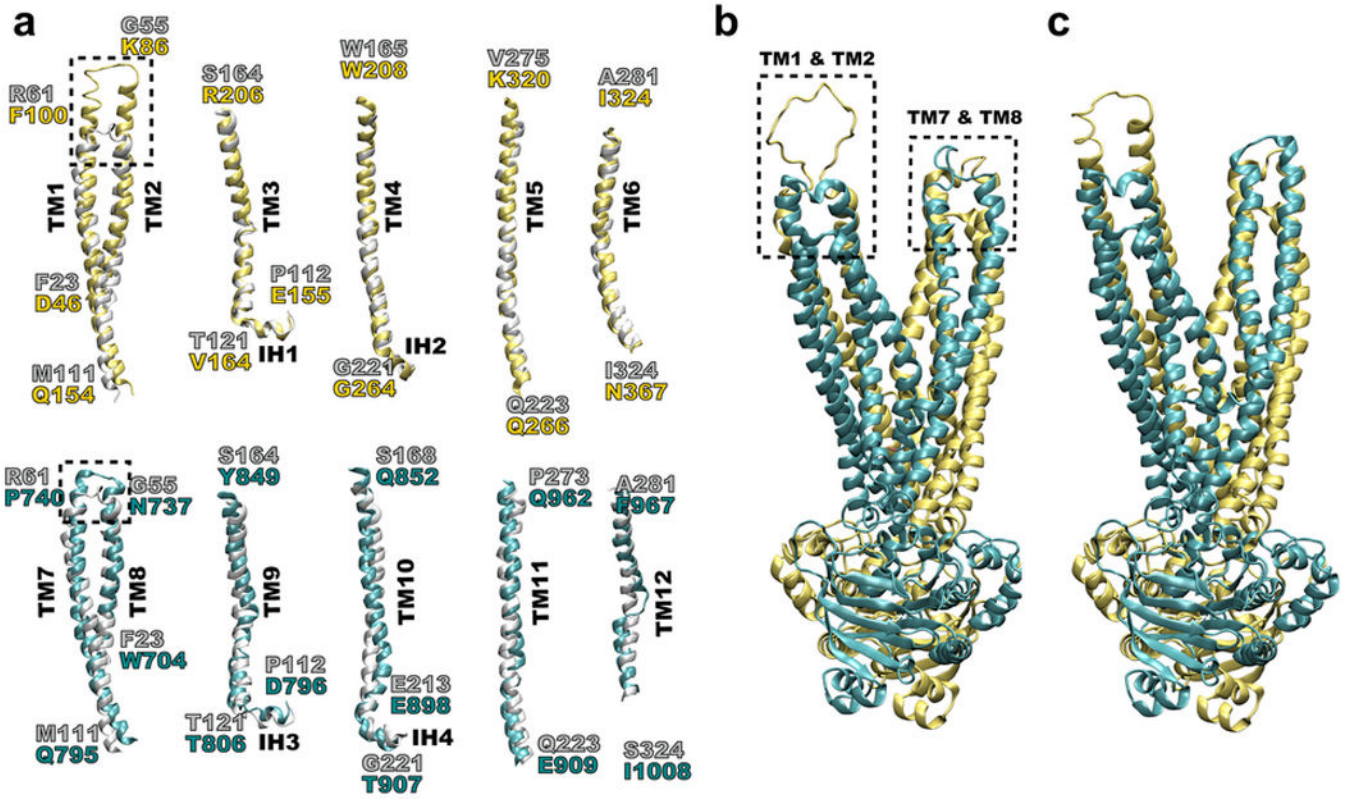

Extended Data Figure 7. Structural modeling of the unknown OF state

(a) Structural alignment of all the TM helices between mouse Pgp and MsbA, which is used as a structural template in model construction. Regions highlighted with black dashed boxes indicate the missing structural segments from the template. TM helices of MsbA are colored silver whereas TM helices 1-6 and 7-12 of Pgp are colored yellow and cyan, respectively. The residues of TM helices and intracellular helices (IH) are labeled in colors corresponding to their structures. (b) Incomplete model of Pgp OF state resulted from the alignment without fixing the missing segments. Incomplete structural regions are highlighted in black dashed boxes. (c) A complete model of Pgp OF state after rebuilding the incomplete regions with structural information obtained from the IF crystal structure of mouse Pgp (PDB accession 4M1M).

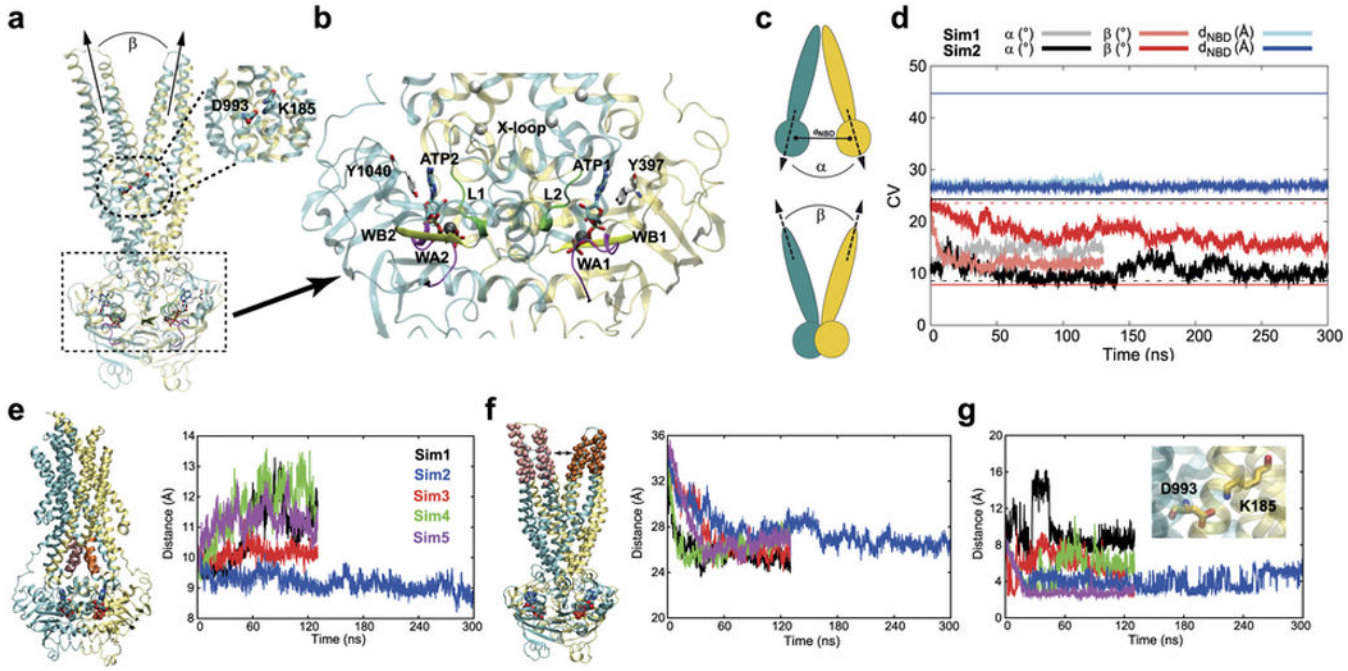

Extended Data Figure 8. Description of the collective variables (CV) used to obtain a reliable OF state of Pgp (a-d) and tracking important structural features to verify the stability of the OF state (e-g)

(a) Orientation quaternion (β) describing the angle between the two bundles of TM helices that separate to form the OF state. Distance between K185 and D993, a charged residue pair located within the translocation chamber. (b) CVs used to form accurate NBD-based interactions, which include NBD-ATP interactions and X-loop interactions. Walker A (WA1 and WA2), Walker B (WB1 and WB2), and LSGGQ (L1 and L2) motifs are shown in purple, yellow, and green new cartoon representations, respectively. Y397/1040 from the A-loop (white) and ATPs (cyan) are shown in stick representations, whereas Mg^{2+} ions and Cα carbons of X-loop residues are displayed as grey and white beads, respectively. (c) Metrics used in evaluating the basic structural elements that are key to any OF ABC exporter, namely, dimerized NBDs (dNBD), closed cytoplasmic (α), and opened extracellular/periplasmic (β) sides. (d) Sim1 (light colors) failed to maintain these basic structural requirements within 10 ns, whereas Sim2 (dark colors) results in a stable OF state for up to 300 ns. Solid and dotted horizontal lines represent the corresponding values in IF and OF conformations, respectively, based on crystal structures of Pgp (PDB accession 4M1M) and MsbA (PDB accession 3B60). (e) Description and time series of center of mass distance between extended TM helical regions of TM3 (V164-V175) and TM10 (E887-E898) shown in orange, and TM4 (A244-A255) and TM9 (T806-D817) shown in pink, describing the tight closing of cytoplasmic side. (f) Description and time series of center of mass distance between the residues forming top half of TMDs that open at the extracellular side (shown with pink and orange beads). (g) Salt bridge interaction between K185 (TM3) and D993 (TM12). These calculations are compared between five different simulations.

Extended Data Table 1

List of collective variables used in non-equilibrium simulations.

Atom1			Atom2	
Residue/Name	**Atom/Group**	**Distance (Å)**	**Residue/Name**	**Atom/Group**
***NBD** (LSGGQ-ATP)				
G530/1175	N	2.76	ATP	O1G
S528/1173	OG	2.88	ATP	O1G
S528/1173	OG	3.30	ATP	03B
Q531/1176	OE1	2.80	ATP	02′
L527/L1172	CA	4.21	ATP	C8
TMD-NBD (X-loop)				
D163	CA	6.0	K1167	CA
E522	CA	6.0	T806	CA
Salt bridge				
K185	NH3	3.2	D993	o=c=o
TMD-based				
β1	TM1, 2, 9 - 12			
β2	TM3-8			

Extended Data Table 2

Details of the five simulations performed in the present study with different combinations of CVs. Simulation was extended until 300 ns for Sim2 upon observing stable OF state.

System	Collective variables			Simulation Time (ns)
	NBD-based	TMD-based	Salt Bridge	
Sim1	+	-	-	130
Sim2	+	+	+	300
Sim3	+	+	-	130
Sim4	+	—	+	130
Sim5	-	+	+	130

Supplementary Material

Refer to Web version on PubMed Central for supplementary material.

Acknowledgments

We thank Richard Stein for advice on the global analysis of DEER data, Professor Ina L. Urbatsch for generous donation of *P. pastoris* expression construct, and Professor Stephan Wilkens for providing three expressed mutants (615-1276, 627-1260 and 613-1258) in *P. pastoris*. This work was supported by National Institutes of Health grants U54-GM087519 (to H.S.M., R.K.N., and E.T.) and P41- GM104601 (to E.T.). We also acknowledge computing resources provided by Blue Waters at NCSA, DOE INCITE, and XSEDE (grant TG-MCA06N060 to E.T.).

References

1. Higgins CF, Linton KJ. The ATP switch model for ABC transporters. Nat Struct Mol Biol. 2004; 11:918–926. [PubMed: 15452563]
2. Rees DC, Johnson E, Lewinson O. ABC transporters: the power to change. Nat Rev Mol Cell Biol. 2009; 10:218–227. [PubMed: 19234479]
3. Jones PM, George AM. Mechanism of the ABC transporter ATPase domains: catalytic models and the biochemical and biophysical record. Crit Rev Biochem Mol Biol. 2013; 48:39–50. [PubMed: 23131203]
4. Sharom FJ. ABC multidrug transporters: structure, function and role in chemoresistance. Pharmacogenomics. 2008; 9:105–127. [PubMed: 18154452]
5. Mchaourab HS, Steed PR, Kazmier K. Toward the fourth dimension of membrane protein structure: insight into dynamics from spin-labeling EPR spectroscopy. Structure. 2011; 19:1549–1561. [PubMed: 22078555]
6. Jeschke G. DEER distance measurements on proteins. Annu Rev Phys Chem. 2012; 63:419–446. [PubMed: 22404592]
7. Gottesman MM, Fojo T, Bates SE. Multidrug resistance in cancer: role of ATP- dependent transporters. Nat Rev Cancer. 2002; 2:48–58. [PubMed: 11902585]
8. Sharom FJ, Yu X, Chu JWK, Doige CA. Characterization of the ATPase activity of P-glycoprotein from multidrug-resistant Chinese hamster ovary cells. Biochem J. 1995; 308:381–390. [PubMed: 7772017]
9. Urbatsch IL, Sankaran B, Weber J, Senior AE. P-glycoprotein is stably inhibited by vanadate-induced trapping of nucleotide at a single catalyitc site. J Biol Chem. 1995; 270:19383–19390. [PubMed: 7642618]
10. Kerr KM, Sauna ZE, Ambudkar SV. Correlation between steady-state ATP hydrolysis and vanadate-induced ADP trapping in Human P-glycoprotein. Evidence for ADP release as the rate-limiting step in the catalytic cycle and its modulation by substrates. J Biol Chem. 2001; 276:8657–8664. [PubMed: 11121420]
11. Ward A, Reyes CL, Yu J, Roth CB, Chang G. Flexibility in the ABC transporter MsbA: Alternating access with a twist. Proc Natl Acad Sci U S A. 2007; 104:19005–19010. [PubMed: 18024585]
12. Zou P, Bortolus M, Mchaourab HS. Conformational cycle of the ABC transporter MsbA in liposomes: detailed analysis using double electron-electron resonance spectroscopy. J Mol Biol. 2009; 393:586–597. [PubMed: 19715702]
13. Aller SG, et al. Structure of P-glycoprotein reveals a molecular basis for poly-specific drug binding. Science. 2009; 323:1718–1722. [PubMed: 19325113]
14. Li J, Jaimes KF, Aller SG. Refined structures of mouse P-glycoprotein. Protein Sci. 2014; 23:34–46. [PubMed: 24155053]
15. Jin MS, Oldham ML, Zhang Q, Chen J. Crystal structure of the multidrug transporter P-glycoprotein from *Caenorhabditis elegans*. Nature. 2012; 490:566–569. [PubMed: 23000902]
16. Verhalen B, Wilkens S. P-glycoprotein retains drug-stimulated ATPase activity upon covalent linkage of the two nucleotide binding domains at their C-terminal ends. J Biol Chem. 2011; 286:10476–10482. [PubMed: 21278250]
17. Holland IB, Blight MA. ABC-ATPases, adaptable energy generators fuelling transmembrane movement of a variety of molecules in organisms from bacteria to humans. J Mol Biol. 1999; 293:381–399. [PubMed: 10529352]
18. Dawson RJ, Locher KP. Structure of a bacterial multidrug ABC transporter. Nature. 2006; 443:180–185. [PubMed: 16943773]
19. Ambudkar SV, Kim IW, Xia D, Sauna ZE. The A-loop, a novel conserved aromatic acid subdomain upstream of the Walker A motif in ABC transporters, is critical for ATP binding. FEBS Lett. 2006; 580:1049–1055. [PubMed: 16412422]
20. Carrier I, Julien M, Gros P. Analysis of catalytic carboxylate mutants E552Q and E1197Q suggests asymmetric ATP hydrolysis by the two nucleotide-binding domains of P-glycoprotein. Biochemistry. 2003; 42:12875–12885. [PubMed: 14596601]

21. Sauna ZE, Müller M, Peng XH, Ambudkar SV. Importance of the Conserved Walker B Glutamate Residues, 556 and 1201, for the Completion of the Catalytic Cycle of ATP Hydrolysis by Human P-glycoprotein (ABCB1). Biochemistry. 2002; 41:13989–14000. [PubMed: 12437356]
22. Tombline G, et al. Properties of P-glycoprotein with mutations in the “catalytic carboxylate” glutamate residues. J Biol Chem. 2004; 279:46518–46526. [PubMed: 15326176]
23. Tombline G, Bartholomew LA, Urbatsch IL, Senior AE. Combined mutation of catalytic glutamate residue in the two nucleotide binding domains of P-glycoprotein generates a conformation that binds ATP and ADP tightly. J Biol Chem. 2004; 279:31212–31220. [PubMed: 15159388]
24. Tombline G, Senior AE. The occluded nucleotide conformation of P-glycoprotein. J Bioenerg Biomembr. 2005; 37:497–500. [PubMed: 16691489]
25. Senior AE, Al-Shawi MK, Urbatsch IL. The catalytic cycle of P-glycoprotein. FEBS Lett. 1995; 377:285–289. [PubMed: 8549739]
26. Siarheyeva A, Liu R, Sharom FJ. Characterization of an asymmetric occluded state of P-glycoprotein with two bound nucleotides: implications for catalysis. J Biol Chem. 2010; 285:7575–7586. [PubMed: 20061384]
27. Moradi M, Tajkhorshid E. Mechanistic picture for conformational transition of a membrane transporter at atomic resolution. Proc Natl Acad Sci U S A. 2013; 110:18916–18921. [PubMed: 24191018]
28. Wen PC, Verhalen B, Wilkens S, Mchaourab HS, Tajkhorshid E. On the origin of large flexibility of P-glycoprotein in the inward-facing state. J Biol Chem. 2013; 288:19211–19220. [PubMed: 23658020]
29. Mishra S, et al. Conformational dynamics of the nucleotide binding domains and the power stroke of a heterodimeric ABC transporter. Elife. 2014:e02740. [PubMed: 24837547]
30. Tombline G, et al. Expression, purification, and characterization of cysteine-free mouse P-glycoprotein. Arch Biochem Biophys. 2006; 445:124–128. [PubMed: 16343415]
31. Smriti, Zou P, Mchaourab HS. Mapping daunorubicin-binding sites in the ATP- binding cassette transporter MsbA using site-specific quenching by spin labels. J Biol Chem. 2009; 284:13904–13913. [PubMed: 19278995]
32. Jeschke G, Polyhach Y. Distance measurements on spin-labelled biomacromolecules by pulsed electron paramagnetic resonance. Phys Chem Chem Phys. 2007; 9:1895–1910. [PubMed: 17431518]
33. Polyhach Y, Bordignon E, Jeschke G. Rotamer libraries of spin labelled cysteines for protein studies. Phys Chem Chem Phys. 2011; 13:2356–2366. [PubMed: 21116569]
34. Eswar N, et al. Comparative protein structure modeling using MODELLER. Curr Protoc Protein Sci. 2007:9. Chapter 2 Unit 2.
35. Simossis VA, Heringa J. PRALINE: a multiple sequence alignment toolbox that integrates homology-extended and secondary structure information. Nucleic Acids Res. 2005; 33:W289–294. [PubMed: 15980472]
36. Pirovano W, Feenstra KA, Heringa J. PRALINETM: a strategy for improved multiple alignment of transmembrane proteins. Bioinformatics. 2008; 24:492–497. [PubMed: 18174178]
37. Zaitseva J, Jenewein S, Jumpertz T, Holland IB, Schmitt L. H662 is the linchpin of ATP hydrolysis in the nucleotide-binding domain of the ABC transporter HlyB. EMBO J. 2005; 24:1901–1910. [PubMed: 15889153]
38. Phillips JC, et al. Scalable molecular dynamics with NAMD. J Comput Chem. 2005; 26:1781–1802. [PubMed: 16222654]
39. Huang J, MacKerell AD Jr. CHARMM36 all-atom additive protein force field: validation based on comparison to NMR data. J Comput Chem. 2013; 34:2135–2145. [PubMed: 23832629]
40. Feller SE, MacKerell AD Jr. An improved empirical potential energy function for molecular simulations of phospholipids. J Phys Chem B. 2000; 104:7510–7515.
41. Foloppe N, MacKerell AD Jr. All-atom empirical foce field for nucleic acids: I. parameter optimization based on small molecule and condensed phase macromolecular target data. J Comput Chem. 2000; 21:86–104.
42. Jo S, Kim T, Im W. Automated builder and database of protein/membrane complexes for molecular dynamics simulations. PLoS One. 2007; 2:e880. [PubMed: 17849009]

43. Jo S, Lim JB, Klauda JB, Im W. CHARMM-GUI Membrane Builder for mixed bilayers and its application to yeast membranes. Biophys J. 2009; 97:50–58. [PubMed: 19580743]

44. Wu EL, et al. CHARMM-GUI Membrane Builder toward realistic biological membrane simulations. J Comput Chem. 2014; 35:1997–2004. [PubMed: 25130509]

45. Jo S, Kim T, Iyer VG, Im W. CHARMM-GUI: a web-based graphical user interface for CHARMM. J Comput Chem. 2008; 29:1859–1865. [PubMed: 18351591]

46. Brooks BR, et al. CHARMM: the biomolecular simulation program. J Comput Chem. 2009; 30:1545–1614. [PubMed: 19444816]

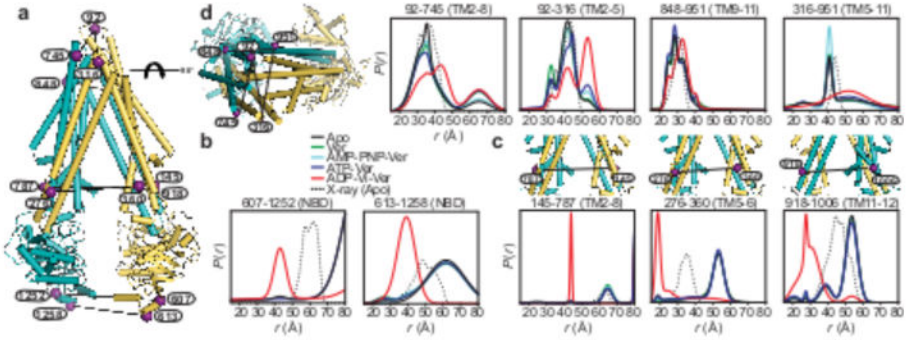

Figure 1. Pgp alternating access

Cartoon representation of Apo Pgp crystal structure (PDB accession 4M1M) with position of spin label pairs represented by spheres (a). Distance distributions in the presence of verapamil (Ver), AMP-PNP/Mg^{2+}/Ver to mimic ATP binding, excess ATP/Mg^{2+}/Ver and ATP/Mg^{2+}/Vi and Ver to trap the transition state of ATP hydrolysis (ADP-Vi-Ver) (b-d). Vanadate-trapping of Pgp (red traces) results in large distance changes in the NBD (b) and the intracellular side of the TMD (c) reflecting a closing movement relative to Apo Pgp while distance distributions for the extracellular region of the TMD (d) are multicomponent and shift to longer distances in the transition state reflecting an opening movement.

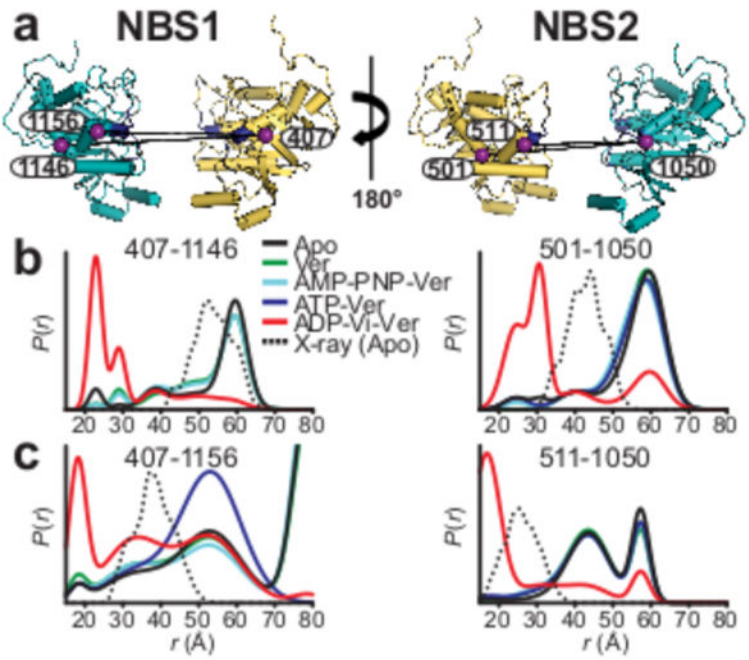

Figure 2. Conformational dynamics of the NBSs

(a) Cartoon representation of the NBSs viewed from the side. Each NBS was monitored by two spin label pairs introduced at structurally equivalent sites. Conserved Walker A and ABC signature motifs are highlighted in dark blue. These spin label pairs (b, c) report distance changes expected from the formation of the NBD dimer in the transition state.

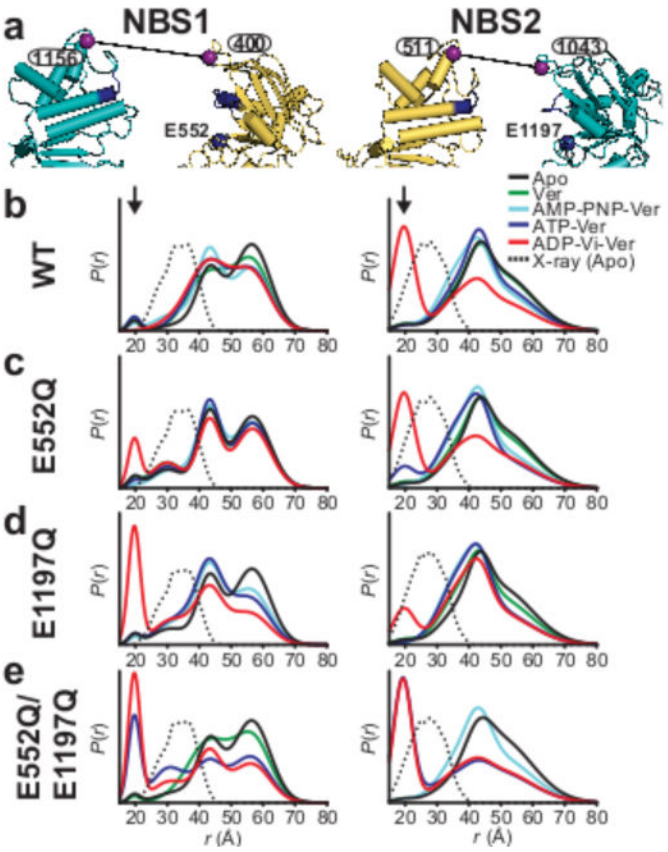

Figure 3. In principle intrinsic local asymmetry at the NBSs reflects catalytic asymmetry

(a) Cartoon representation of the NBSs showing the pairs 400-1156 (NBS1) and 511-1043 (NBS2) represented by purple spheres. Conserved motifs are highlighted in dark blue with the catalytic glutamates represented by blue spheres. A short-distance component is observed in the distribution of the 511-1043 pair monitoring NBS2 but not the 400-1156 pair monitoring NBS1 (b). (c-e) E552Q mutation in NBS1 does not influence the distance distributions substantially (c), while E1197Q inverts the asymmetry in the distance distribution (d). In the double E to Q background, the short distance component is almost equally distributed between the two NBSs and stabilized by ATP/Mg^{2+} (e).

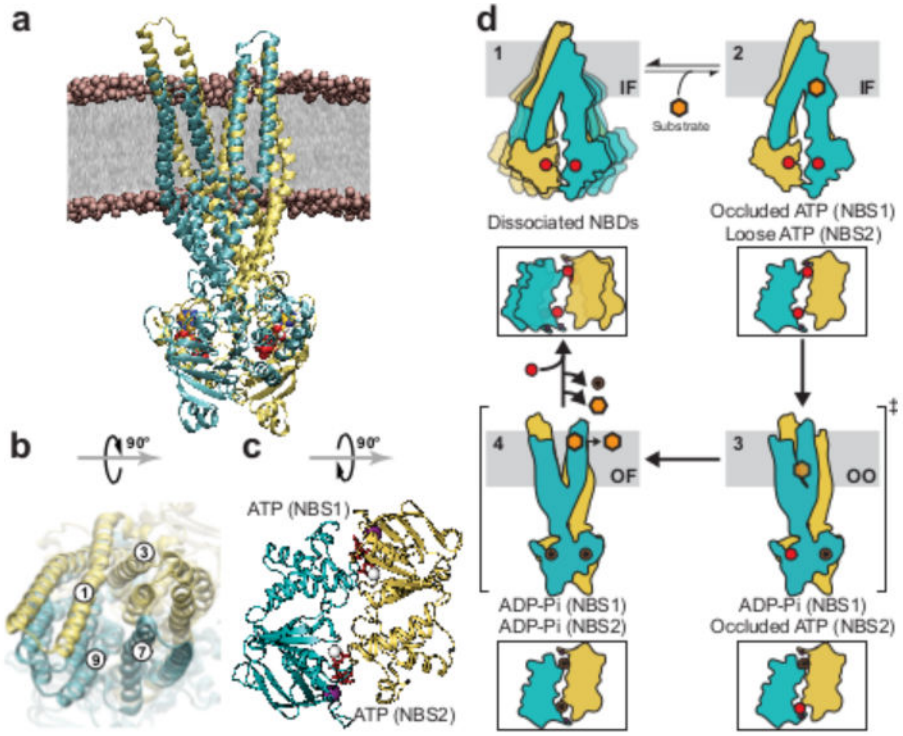

Figure 4. Model of energy input and alternating access in Pgp

(a-c) Different views of the membrane-bound OF state from MD simulations. (a) Side view of the OF state highlighting the extracellular opening of the TMD and dimerization of the NBDs. Two docked Mg^{2+} and ATP molecules are shown in VDW representation. (b) Top down view of the extracellular opening in the modeled OF state. TM helices are labeled to show where the OF separation occurs. (c) Cytoplasmic view of the dimerized NBDs with two docked Mg^{2+} (white spheres) and ATP molecules (red sticks). The conserved tyrosines of the two A-loops are represented as purple spheres. (d) Model of energy transduction by Pgp. 1: Conformational sampling by ATP-bound Pgp enables the NBD to dimerize following the binding of substrate. 2: Previously described conformation that is a precursor to the formation of the transition state where one ATP molecule is occluded. 3: Doubly occluded (OO) transition state following the turnover of one ATP molecule. 4: OF transition state following the hydrolysis of the second ATP molecule. ATP is represented as a red circle, ADP as a brown circle and substrate as an orange hexagon.